

BEAM DYNAMICS SIMULATIONS REGARDING THE EXPERIMENTAL FFAG EMMA, USING THE ON-LINE CODE

Y. Giboudot, Brunel University, Middlesex, D. Kelliher, STFC RAL, Chilton,
F. Méot, CEA & IN2P3 INPG UJF, LPSC, Grenoble, T. Yokoi, John Adams Institute, Oxford.

Abstract

The Electron Model for Many Applications FFAG (EMMA) has been the object of extensive beam dynamics simulations during its design and construction phases, using the ray-tracing code Zgoubi, which has been retained as the on-line simulation engine. On the other hand EMMA commissioning requires further advanced beam dynamics studies as well as on-line and off-line simulations. This contribution reports on some aspects of the studies so performed during the last months using Zgoubi.

INTRODUCTION

Commissioning of EMMA FFAG, constructed at the STFC Daresbury Laboratory in the UK (see companion paper [1]), is now being undertaken, and will be followed by extensive experiments over the coming months.

Numerous numerical experiments have been performed in the recent years based on the use of the stepwise ray-tracing code Zgoubi [2], in support to machine design and beam dynamics studies on the one hand, and on the other hand so to ensure appropriate developments and tests of that code (see companion paper [3]) as it has been retained as the engine for the on-line model of EMMA.

Details on the Zgoubi method can be found in the users' guide [2], its application to all types of FFAG optics is discussed in Ref. [4].

WORKING HYPOTHESIS

In the following, beam dynamics simulations are presented and discussed. They are based on EMMA FFAG ring parameters as displayed in Tab. 1 (Fig. 1). RF cavities are located every two other cell except for two cells which house injection and extraction equipments. Quadrupole magnets are mounted on sliders that allow radial motion, so to allow independent tuning of time of flight and tunes. The RF voltage can be varied, to explore acceleration regimes.

In the following the sole "baseline" geometry will be considered (one of eight different cell tunings designed to assess the various working regimes [5]), QF and QD positioning are $x_D = 34.048$ mm, $x_F = 7.514$ mm.

SIMULATING EMMA CELL

There are various ways to simulate EMMA cell based on numerical procedures available from Zgoubi. The two main classes are analytical models, amongst which : QUADRUPOLE, MULTIPOL, DIPOLES, and field maps,

Table 1: Parameters of EMMA ring, a 42-sided polygon, corners at the long drift - QD interface.

Energy range	MeV	10 - 20
number of turns		<16
circumference	m	16.568
Lattice		F/D doublet
No of cells		42
RF frequency / range	GHz / MHz	1.3 / 5.6
No of RF cavities		19
RF voltage	kV/cavity	20 - 120
<i>EMMA cell</i>		
- cell length	cm	39.448
- length F/D	cm	5.878 / 7.570
- drifts, short/long	cm	5 / 21
- gradient at F/D	T/m	6.695 / 4.704

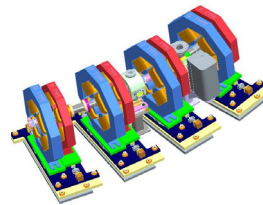


Figure 1: Two EMMA cells.

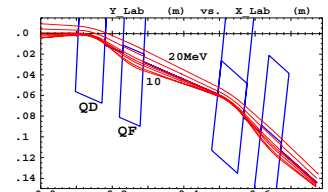


Figure 2: Closed orbits along two cells, "baseline" tuning.

amongst which : TOSCA, EMMA procedures with the particularity as to the latter that it has been installed on purpose [3]. The use of various of these procedures is illustrated below.

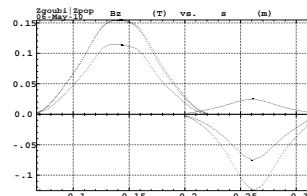


Figure 3: Soft-edge field using MULTIPOL with $B_{dip} \neq 0$, $x_D, x_F = 0$.

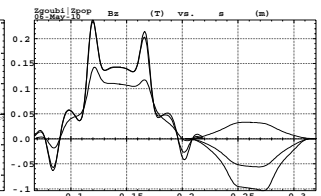


Figure 4: Soft-edge field using MULTIPOL with $B_{dip} = 0$, $x_D, x_F \neq 0$.

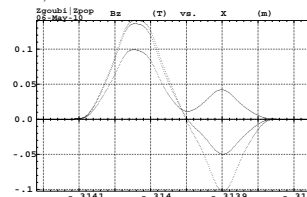


Figure 5: Overlapped soft-edge fields using DIPOLES with $B_{dip} = 0$, $x_D, x_F \neq 0$.

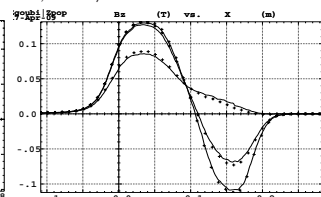


Figure 6: Field across cell, using QF and QD field maps, $E=10, 15$ and 20 MeV.

Table 2: EMMA cell using MULTIPOL procedure.

1	'DRIFT' ld1	
2	6.4009	drift length
3	'MARKER' BPM2 off	
4	'DRIFT' ld2	
5	4.0991	
6	'CHANGREF'	
7	ZR -8.571428571429	reference frame orientation
8	'MULTIPOL' QD	
9	0	
10	7.5699 5.3 -1.601617922.49312 0 0 0 0 0 0 0	length, radius, B_{dip} , B_{quad}
11	0 0 0 0 0 0 0 0 0 0 0 0	fringe lengths, entrance
12	4 0.296571 4.533219 -2.270982 1.068627 0 0.	Enge coefficients
13	0 0 0 0 0 0 0 0 0 0 0 0	fringe lengths, exit
14	4 0.296571 4.533219 -2.270982 1.068627 0 0.	Enge coefficients
15	0 0 0 0 0 0 0 0 0 0 0 0	poles' kew angles
16	0.1	integration step size
17	1 0 0 0.	magnet positioning, Δs , Δx , θ_y
18	'DRIFT' sd	
19	2.689100000000e+00	
20	'MARKER' BPM1 off	
21	'DRIFT' sd	
22	2.310900000000e+00	
23	'MULTIPOL' QF	
24	0	
25	5.8782 3.7 0.5030623 -2.47715 0 0 0 0 0 0 0	
26	0 0 0 0 0 0 0 0 0 0 0 0	
27	4 0.296571 4.533219 -2.270982 1.068627 0 0.	
28	0 0 0 0 0 0 0 0 0 0 0 0	
29	4 0.296571 4.533219 -2.270982 1.068627 0 0.	
30	0 0 0 0 0 0 0 0 0 0 0 0	
31	0.1	
32	1 0 0 0.	magnet positioning, Δs , Δx , θ_y
33	'DRIFT' ld	
34	10.5	
35	'CAVITE' #cav1	
36	7	
37	0 1.300525305355e+09	
38	-6.4e+04 -9.771174812308e+00	
39	'MARKER' BPMCAV	
40	'DRIFT' ld	
41	10.5	

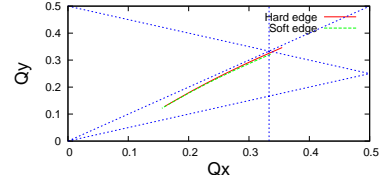


Figure 7: Tune diagram, hard- and soft-edge cases.

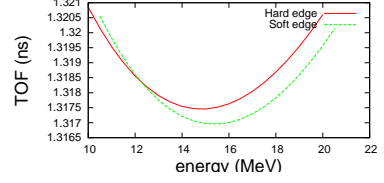


Figure 8: Time of flight, hard- and soft-edge cases.

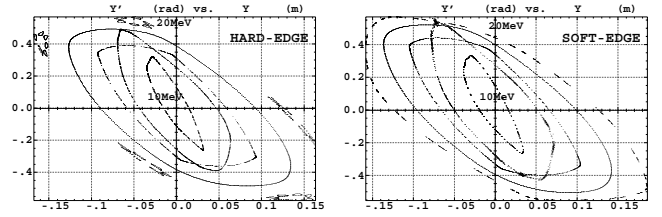


Figure 9: Maximum amplitude, pure horizontal motion.

MULTIPOL Using the MULTIPOL procedure, the input data to Zgoubi for EMMA cells are as displayed in Tab. 2. The field $\vec{B}(s, x, y)$ and derivatives (which the Zgoubi methods needs) are derived from the scalar potential

$$V_n(s, x, y) = (n!)^2 \left\{ \sum_{q=0}^{\infty} (-)^q \frac{\alpha_{n,0}^{(2q)}(s)}{4^q q! (n+q)!} (x^2 + y^2)^q \right\} \times \left\{ \sum_{m=0}^n \frac{\sin(m\frac{\pi}{2}) x^{n-m} y^m}{m! (n-m)!} \right\} \quad (1)$$

n is the multipole order ; s, x, y coordinates are respectively longitudinal, horizontal and vertical ; $\alpha_{n,0}(s)$ is the field fall-off at magnet ends modeled by

$$\alpha_{n,0}(d) = \frac{G_n}{1 + \exp[P(d)]}, \quad P(d) = \sum_{i=0}^5 C_i \left(\frac{d}{\lambda_n}\right)^i$$

with $\alpha_{n,0}^{(2q)} = d^{2q} \alpha_{n,0} / ds^{2q}$; d is the distance to the effective field boundary (EFB) ; $\lambda_n, C_0 - C_5$ are normally determined from prior matching with field fall-off data. In particular $\lambda_1 \approx \text{gapsize}, g$, while $\lambda_n \approx \lambda_1 / n$; varying λ_n will change the fall-off gradient, not the magnetic length.

In the hard edge model a *first order* correction on the focusing is added at EFBs, under the form of a vertical kick, $\Delta\phi = y * \tan(\mathcal{I}g/\rho) / \rho$, with ϕ the vertical angle of the trajectory, ρ and g the local curvature radius and gap, $\mathcal{I} = \int_{-\infty}^{\infty} B_y(s) (B_0 - B_y(s)) / g B_0^2 ds$. Note that some codes introduce higher order corrections, possibly inducing zero-order (orbit) effects.

In the particular data list above the quadrupole displacements x_D, x_F are set to zero (in lines 17 and 32 for respectively QD and QF) and replaced by non-zero B_{dip} values (lines 10 and 25 ; field shown in Fig.3), which actually does not reproduce the multipole symmetry in the cell. A

correct representation of the symmetry instead is obtained with zero B_{dip} and magnet positioning data lines (17 and 32) set respectively to '2 0. x_D 0.', '2 0. x_F 0.' (field shown in Fig.4). This method has the disadvantage of increasing the extrapolation distance from the multipole axis in Eq. 1, thus causing stronger overshoots of the field and derivatives in fringe field regions.

The illness inherent in field modelling using MULTIPOL however, is in the excessive sharpness of the fringe fall-off. This can hardly be overcome because too long fringe fields would result in excessive extent of the field over the drifts, and long overlapping of QD and QF fields. This can be overcome in the following way.

DIPOLES Using the DIPOLES procedure, the (QD,QF) doublet is described as displayed in Tab. 3. The field

Table 3: EMMA cell using DIPOLES procedure.

1	'CHANGREF'	
2	0 0. -8.485714285714285714	reference frame orientation
3	'DIPOLES'	
4	0	
5	2 0.0225349 1e5	# of magnets, AT, RM
6	0.008117479 0. 1.50161792 1 -29371.7889 0 0 0 0.	$\theta_{ref}, x_D, B_0, 1,$
7	3 0 EFB 1	
8	4 -1.455 2.2670 -6395 1.1558 0 0 0.	
9	+0.0021686166 0 1.E6 -1.E6 1.E6 1.E6	
10	3 0. EFB 2	
11	4 -1.455 2.2670 -6395 1.1558 0 0 0.	
12	-0.0021686166 0 1.E6 -1.E6 1.E6 1.E6	
13	0 0. EFB 3	
14	0 0 0 0 0 0 0 0.	
15	0 0 0 0 0 0 0 0.	
16	0.0148348649 0 -50302885 1 -133090. 0 0 0 0.	$\theta_{ref}, x_D, B_0, 1,$
17	3 0 EFB 1	
18	4 -1.455 2.2670 -6395 1.1558 0 0 0.	
19	0.00168398 0 1.E6 -1.E6 1.E6 1.E6	
20	3 0. EFB 2	
21	4 -1.455 2.2670 -6395 1.1558 0 0 0.	
22	-0.00168398 0 1.E6 -1.E6 1.E6 1.E6	
23	0 0. EFB 3	
24	0 0 0 0 0 0 0 0.	
25	0 0 0 0 0 0 0 0.	
26	2 100 KIRD, Resol	
27	.1	
28	2 99998.43505620515017 -8.78495e-05 1e5 8.78495e-05	

$\vec{B}(s, x, y)$ due to N magnets ($N = 2$ here) is extrapolated from the vertical component (field shown in Fig.5)

$$B_z = B_{z0,i} + \sum_{i=1}^N [\mathcal{F}_i(R, \theta) \sum_{m=1}^M b_{m_i} (R - RM_i)^m]$$

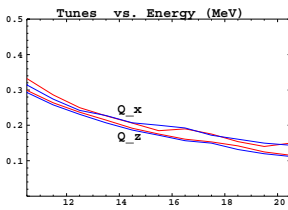


Figure 10: Tunes versus energy, “D&F” (blue, thick lines) and “D+F” (red, thin lines).

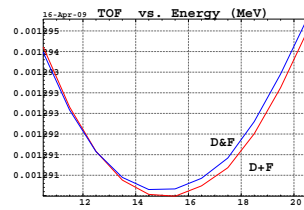


Figure 11: Time of flight parabola, “D&F” (blue, thick line), “D+F” (red, thin line).

Figs. 7, 8 show tunes and TOF respectively, in both cases of hard-edge and of fringe field models. Fig. 9 shows typical maximum stable amplitude phase-spaces.

FIELD MAPS Given the complexity of EMMA cell (i.e., essentially (i) the absence of flat top in the quadrupoles (Figs. 3-6), (ii) the difficulty of correct field simulation at large beam excursion in the quadrupole openings), analytical models have their limits, a true representation of the cell can only rely on field maps.

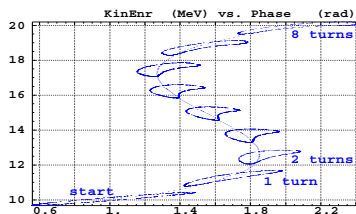


Figure 12: Serpentine motion of a hollow bunch in longitudinal phase-space, from 10 to 20 MeV.

It has been shown [6] that the quadrupole doublet can be represented with good precision with QF and QD field maps generated independently and superimposed. Fig. 6 shows typical field across the cell so obtained. Figs. 10, 11 show resulting tunes and time of flight with two different methods: QD and QF doublet represented with either a single field map containing both quads (“D&F” case) or with two independent field maps superimposed (“D+F” case).

What precedes may be considered to raise the question of the comparison of simulation methods and codes. Work has been done on that, details can be found in [9].

ACCELERATION

Rapid acceleration is based on a method of “serpentine” - quasi-isochronous - phase space configuration, a major objective in the EMMA method. This is illustrated in Fig. 12 which displays 8-turn acceleration in EMMA 42-cell ring, with one 1.3 GHz, $\hat{V} \approx 64$ kV RF cavity every two cells except for two cells in the injection and extraction regions (Fig. 13-left).

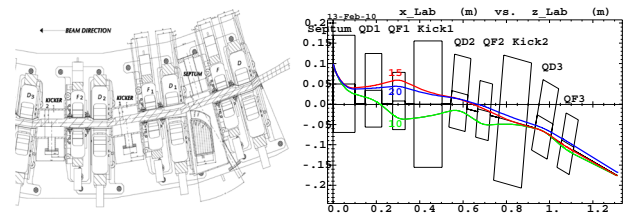


Figure 13: Injection section and 12 MeV orbits.

INJECTION/EXTRACTION

The injection section is sketched in Fig. 13. A series of three successive cells house respectively the injection septum and two kickers. For all injected energy, the appropriate range of values of these three variables is derived by matching given a series of constraints: closed orbit coordinates downstream of the second kicker, maximum septum field in $[-0.7, 0.7]$ kG, geometrical acceptance of the vacuum pipe. Fig. 13 sketches typical results so obtained [8].

The extraction section has the same arrangement, in reverse order, analogous working constraints and extraction paths.

VIRTUAL EMMA

Full acceleration simulation cycles, including injection line into and extraction line from the ring, have been performed using both analytical or field map modelling of the cell doublet. Detailed description can be found in Ref. [7].

REFERENCES

- [1] The EMMA Non-scaling FFAG, T.R. Edgecock et al., these proceedings.
- [2] The ray-tracing code Zgoubi, F. Méot, NIM-A 427 (1999) 353-356; Zgoubi users' guide, F. Méot, S. Valero, CEA DSM DAPNIA/SEA-97-13 (1997); <http://sourceforge.net/projects/zgoubi/>
- [3] Recent Developments On The EMMA On-Line Commissioning Software, Y. Giboudot et al., THPD024, these proceedings.
- [4] Beam dynamics simulations in FFAGs using Zgoubi, F. Méot, BD-Newsletter 43, (Aug. 2007) 47-54.
- [5] The EMMA Main Ring Lattice, J.S. Berg, Nucl. Instrum. Methods A 596 (2008) 276-284.
- [6] Optical matching of EMMA cell parameters using field map sets, Y. Giboudot, F. Méot, Procs. PAC 09, Vancouver.
- [7] Virtual EMMA using Zgoubi, F. Méot, EMMA commissioning workshop, Daresbury, Dec. 2009.
- [8] Injection into EMMA, septum and kicker tunings, F. Méot, rep. LPSC-10-24 (2010); Simulation of injection into EMMA, injection section, F. Méot, rep. LPSC-10-33 (2010).
- [9] Comparison of EMMA Parameter Predictions, E. Keil, CERN-BE-2010-006 (2010); M. Craddock et al., THPD022, these proceedings.